A quenchable superhard carbon phase synthesized by cold compression of carbon nanotubes

Zhongwu Wang[†‡], Yusheng Zhao[†], Kimberly Tait[†§], Xiaozhou Liao[†], David Schiferl[†], Changsheng Zha[¶], Robert T. Downs[§], Jiang Qian[†], Yuntian Zhu[†], and Tongde Shen[†]

[†]Los Alamos National Laboratory, Los Alamos, NM 87545; [§]Department of Geosciences, University of Arizona, Tucson, AZ 85721; and [¶]Cornell High Energy Synchrotron Source, Wilson Laboratory, Cornell University, Ithaca, NY 14853

Communicated by Russell J. Hemley, Carnegie Institution of Washington, Washington, DC, August 11, 2004 (received for review June 16, 2004)

A quenchable superhard high-pressure carbon phase was synthesized by cold compression of carbon nanotubes. Carbon nanotubes were placed in a diamond anvil cell, and x-ray diffraction measurements were conducted to pressures of ≈100 GPa. A hexagonal carbon phase was formed at ≈75 GPa and preserved at room conditions. X-ray and transmission electron microscopy electron diffraction, as well as Raman spectroscopy at ambient conditions, explicitly indicate that this phase is a sp^3-rich hexagonal carbon polymorph, rather than hexagonal diamond. The cell parameters were refined to $a_0 = 2.496(4)$ Å, $c_0 = 4.123(8)$ Å, and $V_0 = 22.24(7)$ Å ^{3}. There is a significant ratio of defects in this nonhomogeneous sample that contains regions with different stacking faults. In addition to the possibly existing amorphous carbon, an average density was estimated to be 3.6 ± 0.2 g/cm^3, which is at least compatible to that of diamond (3.52 g/cm^3). The bulk modulus was determined to be 447 GPa at fixed $K' \equiv 4$, slightly greater than the reported value for diamond of ≈440–442 GPa. An indented mark, along with radial cracks on the diamond anvils, demonstrates that this hexagonal carbon is a superhard material, at least comparable in hardness to cubic diamond.

The flexibility of carbon to form *sp*-, sp^2-, and sp^3-hybridized bonds results in numerous phases such as graphite, polymeric-fullerences, nanotubes, and cubic and hexagonal diamonds (1). The carbon polymorphs, other than hexagonal and cubic diamond, have been observed to transform to an unquenchable high-pressure phase under cold compression (1–4). The phase can be brought to room pressure if the temperature is kept <100 K, but it reverses when the temperature is raised back to room conditions (1). It has been assumed that this high-pressure phase either exhibits a hexagonal structure or it is amorphous. With *in situ* heating under pressure, this carbon phase transforms to cubic diamond (2, 3, 5). Numerous studies have been performed to accurately explore its structural characteristics, but the question remains as to whether this phase is a newly discovered hexagonal carbon or the previously known hexagonal diamond. Unfortunately, characterizing the hexagonal phase as hexagonal diamond has been based only on the extrapolation of the high-pressure data from the hexagonal phase to room conditions, and comparing the extrapolated data to that observed in natural hexagonal diamond, lonsdaleite, from a meteorite (2, 3). Hexagonal diamond should exhibit a distinctive Raman active mode at ≈1,310 cm^{-1} (6, 7), but no investigation has been performed on synthesized samples that combines both x-ray diffraction and Raman spectroscopy to show whether the hexagonal carbon is, in fact, hexagonal diamond or not.

Most recently, a carbon phase that is intermediate between graphite and cubic diamond was observed at a pressure of 20 GPa by using graphite powder as starting material that is capable of indenting diamond (8). Synchrotron x-ray inelastic scattering revealed that half of the π-bonds between the carbon sheets in graphite appear to transform to σ-bonds, and therefore, the intermediate phase could not be hexagonal diamond. It was concluded that the intermediate phase is a distinct phase of carbon. X-ray diffraction was not of sufficient quality to provide a precise structural determination; however, pressure-induced peak splitting suggests that the observed intermediate phase exhibits either orthorhombic or monoclinic symmetry. The intermediate phase is not quenchable and reverses to graphite, so it has only low potential for industrial application.

In this article, we describe the synthesis of a quenchable high-pressure hexagonal carbon phase formed by the cold compression of carbon nanotubes. An obvious indentation-induced mark displaying linear radial cracks on the diamond anvils, similar to that made in general hardness measurements, unambiguously demonstrates that the observed phase has a hardness at least comparable to that of cubic diamond. Moreover, we provide x-ray and high-resolution transmission electron microscopy (TEM) along with electron diffraction and Raman spectroscopic data that clearly confirm that this phase is a hexagonal carbon polymorph and not hexagonal diamond. Because this phase can be quenched to room conditions, it also cannot be the intermediate phase.

The carbon nanotubes used in this study have tube diameters ranging from 1.8 to 5.1 nm, as shown in high-resolution TEM images (Fig. 1 *A* and *A′*). High-pressure x-ray diffraction measurements were performed at room temperature by using a gasketed high-pressure diamond anvil cell (9). A mixture of ≈96% carbon nanotube and ≈4% platinum without pressure medium was placed in a T301 steel gasket hole, 70 μm in initial thickness and 80 μm in diameter. Platinum served as a pressure calibrant. Energy-dispersive synchrotron radiation at the Cornell High Energy Synchrotron Source was used for x-ray diffraction measurements. Energy calibrations used the well known radiation sources (^{55}Fe and ^{133}Ba), and angle calibrations at $2\theta = 11°$ were made from the six peaks of standard Au powder. Powder x-ray diffraction patterns were collected at pressures to ≈100 GPa for refinement of cell parameters and determination of the newly formed phase. Raman spectroscopy and TEM electron diffraction were also used to check the structural characteristics of the starting and recovered samples.

The x-ray diffraction pattern collected at ambient conditions at the beginning of the experiment exhibits quite broad peaks (Fig. 2), which are typical for the nano-sized particles of carbon nanotubes. On elevation of pressure, combination of the size- and strain-induced effects led to an obvious further broadening of the observed x-ray diffraction peaks. Above 60 GPa, the diffraction peaks from the sample became indistinguishable from each other. It is noticeable that, below 60 GPa, the diffraction peaks display a significant shift to higher energy, implying that carbon nanotube has high compressibility. Above 75 GPa, the diffraction peaks of carbon nanotubes were no longer observable, but a slight rotation of the pressure-lever screw resulted in a remarkable jump in pressure. We suggest that, at 75 GPa, a denser phase with greater incompressibility started

Abbreviation: TEM, transmission electron microscopy.

[‡]To whom correspondence should be addressed. E-mail: z_wang@lanl.gov.

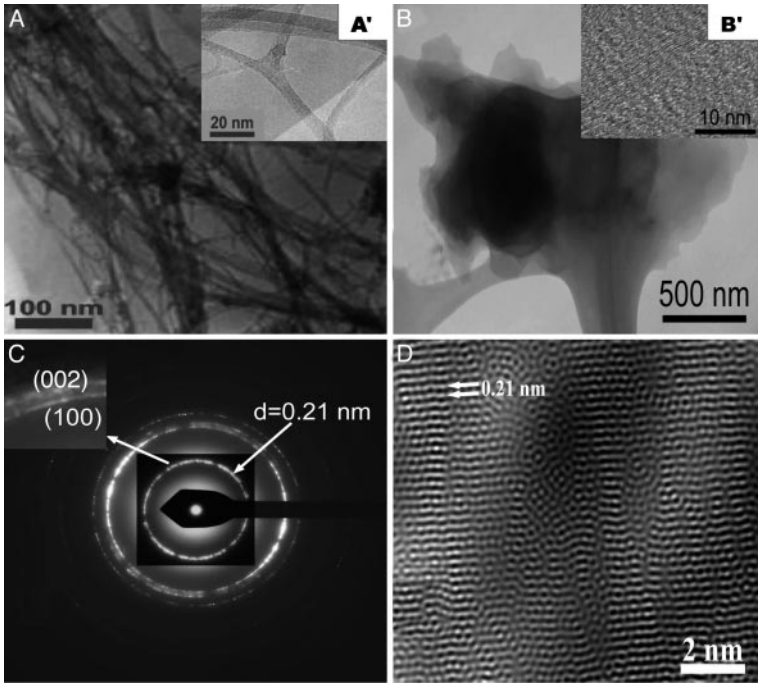

Fig. 1. TEM images of starting and recovered carbon nanotubes assembled into bundles. (*A* and *A′*) Low- and high-magnification images of the starting carbon nanotubes, showing the wall *d*-spacing of 0.34 nm in *A′*. (*B* and *B′*) The compact morphology of the recovered sample shows that carbon nanotube characteristics still remained at the edge of the sample. (*C*) Electron diffraction pattern that indicates a hexagonal structure (a_0 = 0.24 nm, c_0 = 0.43 nm), differing from graphite in which the strongest peak, (002) with *d*-spacing 0.34 nm, should be observed. (*D*) Filtered high-resolution TEM image of the hexagonal carbon polymorph. Highly imperfect fringes with lattice distances of 0.21 nm and hexagonal structural morphologies are clearly seen.

to form. Upon release of pressure, we observed several peaks that differed from those observed in the unquenchable hexagonal carbon formed from graphite by cold compression at ≈20 GPa (3). At zero pressure, after removing the sample from the diamond anvil cell, a high-quality x-ray diffraction pattern was obtained (Fig. 2). The pattern was indexed with hexagonal symmetry (Table 1), and cell parameters were refined to a_0 = 2.496(4) Å, c_0 = 4.123(8) Å, and V_0 = 22.24(7) Å^3. This cell volume is somewhat smaller than those observed for hexagonal diamond or extrapolated from hexagonal carbon (2, 3). Correlating particle size with the observed intensity ratio of the two observed Raman peaks {grain size (nm) = $100/[22.9*(I_D/I_G)]$} (e.g., Raman modes D and G in Fig. 3) (4), we estimated that the particle size of recovered sample is ≈5.2 nm. Nanosize-induced contraction (9) may slightly affect the cell volume and structure, but it is unlikely to result in such a remarkable volumetric change. Under uniaxial compression, the carbon nanotubes quickly developed strong preferred orientation with the *c*-axis parallel to the diamond anvil cell axis (10), which correspondingly led to a significant decrease in the intensity of the (002) peak and increase in the intensity of the (100) peak of carbon nanotube (3). As for the recovered hexagonal carbon, we observed that the corresponding (002) plane displayed the greatest intensity among all observed diffraction peaks. Thus, we conclude that the *c*-axis of the hexagonal carbon was genetically transformed from the *c*-axis of the carbon nanotube. This finding is not consistent with observations from previous studies from the unquenchable hexagonal carbon formed from graphite by cold compression (2, 3). Based on the peak reflections and extinction rules for (*00l*) and (*h0l*) and (*hhl*) in which $l = 2n$, the structural symmetry of the carbon phase can be restricted to three possible space groups: $P6_3mc$ (no. 186), $P\bar{6}2c$ (no. 190), and $P6_3/mmc$ (no. 194). The graphite with the symmetry group of $P6_3/mmc$ (no. 194) also allows one to exclude this space group. Although hexagonal diamond was previously indexed to $P6_3/mmc$ (no. 194) (2), we used the reported data (2) and gave the space group of hexagonal diamond as $P6_3mc$ (no. 186), not $P6_3/mmc$ (no. 194). Moreover, in space group 186, the (100) peak should be stronger than the (002) peak. This notion is consistent with the reported x-ray diffraction patterns (2, 3), but different from our x-ray diffraction data. Thus, the space group of $P6_3mc$ (no. 186) can further be excluded from our Raman data and x-ray diffraction pattern (Fig. 2). Therefore, the space group of $P\bar{6}2c$ (no. 190) is the one that best fits the diffraction data.

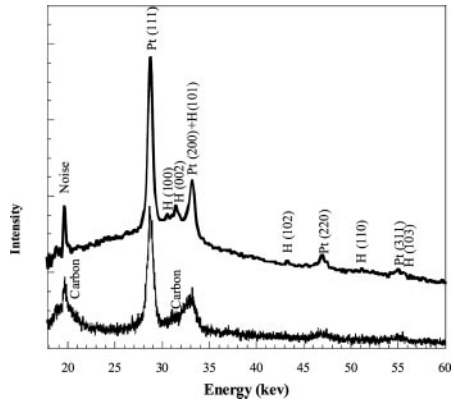

Fig. 2. X-ray diffraction patterns of the starting sample and recovered high-pressure polymorph of nanotube released from ≈100 GPa. The sharp noise is overlapping with the carbon nanotube peak of (002).

Table 1. Observed (obs) and calculated (cal) *d*-spacings of the hexagonal carbon polymorph at ambient conditions

hkl	*d*-spacing (obs), Å	*d*-spacing (cal), Å	Difference, Å
100	2.155	2.161	−0.006
002	2.053	2.061	−0.008
102	1.495	1.492	0.003
110	1.248	1.248	0.000
103	1.161	1.160	0.001

The cell parameters of the hexagonal carbon polymorph are calculated to be a_0 = 2.496(4) Å, c_0 = 4.123(8) Å, and V_0 = 22.24(7) Å^3. Because the peak of H(101) is overlapping with the peak of Pt(200), the corresponding energy value can not be accurately obtained, so we did not use this peak in our calculation.

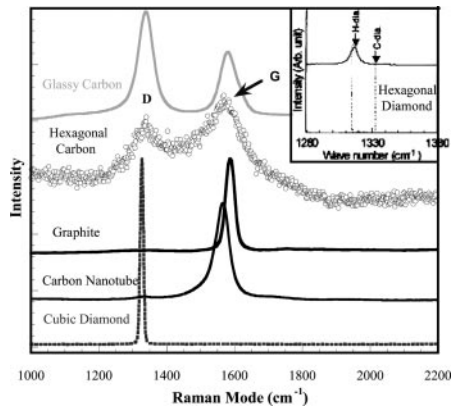

Fig. 3. Raman spectra of several structural polymorphs of carbon collected at ambient conditions. (*Inset*) A representation of the Raman spectrum of hexagonal diamond made by shock-wave impact on diamond (7).

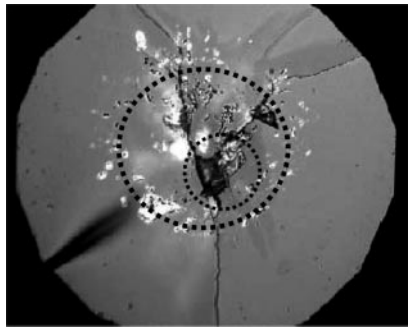

Fig. 5. Photomicrograph showing indentation (crack in center and related radial crack lines) of the diamond anvil by the high-pressure hexagonal polymorph of cold-compressed carbon nanotubes. The large circle represents the gasket hole; the small circle highlights the indentation mark with the depth of ≈3 μm (e.g., estimated from microscopy focusing) at the center of the diamond anvil that has the highest pressure).

Electron diffraction has also strongly confirmed the high-pressure hexagonal carbon polymorph observed from x-ray diffraction investigation (Figs. 1 and 2). High-resolution TEM images further revealed that pressure induced morphological variation of carbon nanotubes. The starting materials exhibited the assembled nanotube bundles (Fig. 1*A*), which have a wall *d*-spacing of 0.34 nm, corresponding to the *d*-spacing of the graphite carbon sheets indexed as the diffraction plane (002) (e.g., Fig. 1*A′*). The recovered hexagonal carbon polymorph displayed compacted and crushed powder characteristics (Fig. 1*B*), but typical nanotube characteristics still remained in small areas (e.g., Fig. 1*B′*), close to the edge of the sample. A possible explanation may be that there is a large pressure gradient across the diamond anvil cell, and sample edges, near the gasket, were never subjected to the same high pressures as the center of the cell. However, the pressure near the gasket was still >70 GPa. Thus, we suggest that, even though a carbon nanotube has very low incompressibility, its strength can still keep its original nature without crushing the tube at least to a pressure of ≈70 GPa (i.e., transition pressure). The electron diffraction pattern of this material is a direct and convincing indication of a hexagonal symmetry (Fig. 1*C*), different from the original hexagonal nanotube structure in which the strongest diffraction peak at $d = 0.34$ nm would be observed. The diffraction line at $d = 0.21$ nm is highly irregular and corresponds to the peaks of (100) and (002) with the *d*-spacings of 0.216 and 0.205 nm, respectively (Table 1). The cell parameters were calculated to be $a_0 = 0.24$ nm and $c_0 = 0.43$ nm, reasonably consistent with those determined from the high-resolution synchrotron x-ray diffraction pattern (Table 1 and Fig. 2). A filtered high-resolution TEM image clearly shows the imperfect lattice fringes with a distance of 0.21 nm and the hexagonal structural characteristics of the high-pressure hexagonal carbon polymorph (Fig. 1*D*). Such a short interlayer distance of 0.21 nm is very close to the self-compression *c*-layer interdistance of 0.22 nm observed in the center of the irradiation-induced carbon onion (11). It is very interesting that the center part of the onion with the *c*-layer interdistance <0.22 nm transforms to diamond at heating above 600°C (11). Thus, this may imply that such a formed hexagonal carbon is the significant step for the transformation of graphite to diamond. The density was calculated to be 3.65 g/cm^3. This carbon phase has a reduced carbon layer distance of 0.21 nm, which is significantly shorter than that of graphite (0.34 nm), but within the carbon sheets; the C—C bond length of 0.143 nm is close to that in graphite (0.141 nm). Moreover, the formed strong bonds in the carbon phase replace the weak van der Waals forces between carbon sheets of graphite and further result in the appearance of the higher coordination number (e.g., ≈5–9) relative to 3 of graphite. Thus, the variation of both bond length and coordination number could lead to a higher density at least locally in the phase. However, there exists a significant ratio of defects and the nonhomogeneous structure that contains different regions with different stacking faults. In addition to the possibly amorphous carbon on the grain boundary, a reduced density of 3.6 ± 0.2 g/cm^3 is reasonably estimated to represent its average density. Thermodynamics dictates that a high-pressure phase be denser than the low-pressure polymorph; the carbon phase clearly has a density slightly higher or at least the same as diamond (3.52 g/cm^3).

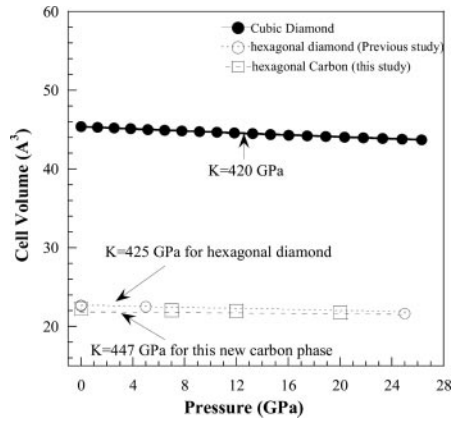

Fig. 4. Comparison of compressibilities between cubic diamond and the observed high-pressure hexagonal carbon. Hexagonal carbon is slightly more incompressible than cubic diamond.

A high-pressure hexagonal phase of carbon has been observed in cold compression of bulk and nanocrystalline graphite (1–4) but has never been preserved at room conditions. However, it is still uncertain whether this phase is really the so-called hexagonal diamond, since no convincing Raman spectrum was collected *in situ* to demonstrate the appearance of the sp^3 vibrational mode at ≈1,310 cm^{-1}, a characteristic signature of hexagonal diamond (6, 7). So far, x-ray diffraction data suggest the existence of the so-called hexagonal diamond (2, 4), but Raman spectroscopic studies performed at similar experimental conditions indicate that the observed hexagonal form is a high-pressure polymorph of carbon (1, 8, 12). Unfortunately, no experiment has combined Raman and x-ray diffraction, so it is impossible to determine whether there is agreement between the previous observations. Since hexagonal diamond obtained by *in situ* heating is assumed to be pressure-quenchable (2, 3, 8), we must consider whether

our hexagonal carbon is, in fact, the hexagonal diamond phase, obtained after having exceeded a critical pressure. We collected ambient condition Raman spectra of various carbon polymorphs, including single-crystal graphite, glassy carbon, starting nanotube, cubic and hexagonal diamond (e.g., induced from cubic diamond by shock impact) (7), and our recovered hexagonal sample (Fig. 3). The spectra of the recovered sample exhibits two broad peaks centered at 1,581 and 1,355 cm^{-1}, respectively, which are characteristics of carbon with a very small particle size (1, 11). Such spectroscopic characteristics are very similar to those of glassy carbon with a significant ratio of sp^3/sp^2 bonding (13), but remarkably different from those of the starting nanotube, single-crystal graphite, or cubic and hexagonal diamond (7). The 1,355-cm^{-1} peak of glassy carbon is much stronger and sharper than that of the recovered hexagonal phase (1). It is also clear that our hexagonal form is not hexagonal diamond, since it should only have a single Raman active mode at $\approx$1,310 cm^{-1}, representing the occurrence of the sp^3-hybridized bonds (6, 7, 12). We therefore conclude that this is an additional high-pressure carbon phase. Moreover, based on the similarity between the Raman spectrum of the material and that of amorphous or nanocrystalline carbon with a large fraction of sp^3 state ($\approx$80–95% of sp^3), it is suggested that the this phase could have a sp^3/sp^2 ratio of $\approx$90%. The remaining sp^2 carbon possibly exists at intergrain boundaries.

The kinetics required to preserve this phase at room conditions still remains unclear. Since this phase results from compressed bundled carbon nanotubes, one significant consideration may be that the combined effect induced by nanotube bonding topology and nanosize plays a critical role in the structural stability of this hexagonal phase. Another consideration is the maximum pressure subjected on the sample. Previous studies of carbon nanotubes have been performed with various techniques to a pressure of 62 GPa (14–17). Although discontinuities in electrical conductivity and vibrational modes have been observed, the similar hardness and bulk modulus of this phase to graphite indicates that no significant structural change took place before 62 GPa (14, 15). Moreover, experiments that observed the unquenchable hexagonal carbon phases were performed only <65 GPa (1, 3, 4, 8, 12). In our study, we observed a significant change in compressibility and a disappearance of diffraction peaks at 75 GPa, which we interpret as indicative of a transformation. Thus, it may be that the sample must be exposed to a critical pressure of at least 75 GPa.

A Birch–Murnaghan equation of state was used to fit the pressure-volume data in this study to 25 GPa, giving a bulk modulus of K = 447 GPa with $K' \equiv 4$ (Fig. 4). The broadening of the diffraction peaks >25 GPa precluded refining reliable cell parameters above this pressure. Our bulk modulus was slightly greater than the observed hexagonal diamond where K = 425 GPa (2, 3). These two studies used incident x-ray beam from different directions, which may result in a slight difference between the two studies. In our study, the x-ray beam was parallel to the compression, which may overestimate the bulk modulus. In previous study, the x-ray beam was vertical to the compression, and the resulting data are close to that obtained at hydrostatic conditions. Because the data were collected only <25 GPa, the error was estimated to be 7%. Therefore, hexagonal carbon appears to be compatible with diamond (K = $\approx$440–442 GPa) (18). However, the bulk modulus does not have a significant correlation to the hardness of materials, and instead, the enhancement of shear modulus results in the increase of hardness (18). As shown in Fig. 5, the hexagonal carbon made a noticeable indentation mark with a crack size of 25 μm, along with several radial linear cracks. These features are similar to indentation-induced crack phenomena found in hardness measurements. Indentation-induced cracks typically take place only when the indented force on the top of the indentator is close to or higher than the hardness of the indented materials. Diamond typically displays a hardness of 80–100 GPa. The diamond in this study was a defect-free single crystal that should have a hardness close to 100 GPa, so the observed crack features at 100 GPa are reasonably understood. Moreover, such an indented characteristic is the same as that obtained by nanocrystalline diamond. Since the nanosize-induced effects can result in a significant increase of hardness and elastic modulus (9, 18), it is accepted that the nanocrystalline diamond has a hardness higher than conventional single crystal diamond. It is noted that recent annealed chemical vapor deposition single crystal diamond has a significantly higher hardness than standard diamond (19). With its density being at least compatible with diamond, we conclude that the hexagonal carbon we observed is a superhard material with a hardness in the range of diamond (>80 GPa). Because this superhard material can be preserved at ambient conditions, technological application in industry is promising.

We thank Dr. Russell Hemley for significant comments, advice, and kind editorial assistance; two reviewers for critical comments and invaluable advice; and the Carnegie/Department of Energy Alliance Center for support. The Director's Postdoctoral Fellowship Fund at Los Alamos National Laboratory supported this work. Part of the work was conducted at the Cornell High Energy Synchrotron Source, which is supported by the National Science Foundation and the National Institutes of Health/National Institute of General Medical Sciences under Award DMR 9713424.

1. Miller, E. D., Nesting, D. C. & Badding, J. V. (1997) *Chem. Mater.* **9,** 18–22.
2. Bundy, F. P. & Kasper, J. S. (1967) *J. Chem. Phys.* **46,** 3437–3443.
3. Yagi, T., Utsumi, W., Yamakata, M., Kikegawa, T. & Shimomura, O. (1992) *Phys. Rev. B Condens. Matter* **44,** 6031–6039.
4. Patterson, J. R., Kudryavtsev, A. & Vohra, Y. K. (2002) *Appl. Phys. Lett.* **81,** 2073–2075.
5. Yusa, H. (2002) *Diam. Relat. Mater.* **11,** 87–91.
6. Wu, B. & Xu, J. (1998) *Phys. Rev. B Condens. Matter* **57,** 13355–13358.
7. He, H., Sekine, T. & Kobayashi, T. (2002) *Appl. Phys. Lett.* **81,** 610–612.
8. Mao, W. L., Mao, H. K., Eng, P. J., Trainor, T. P., Newville, M., Kao, C., Heinz, D. L., Shu, J., Meng, Y. & Hemley, R. J. (2003) *Science* **302,** 425–427.
9. Wang, Z. W., Zhao, Y., Schiferl, D., Zha, C. S., Downs, R. T. & Sekine, T. (2003) *Appl. Phys. Lett.* **83,** 3174–3176.
10. Bendiab, N., Almairac, R., Sauvajol, J. L., Rols, S. & Elkaim, E. (2003) *J. Appl. Phys.* **93,** 1769–1773.
11. Banhart, F. & Ajayan, P. M. (1996) *Nature* **382,** 433–436.
12. Xu, J., Mao, H. K. & Hemley, R. J. (2002) *J. Phys. Condens. Matter* **11,** 11549–11522.
13. Chhowalla, M., Ferrari, A. C., Robertson, J. & Amaratunga, T. (2000) *Appl. Phys. Lett.* **76,** 1419–1421.
14. Patterson, J. R., Vohra, Y. K., Weir, S. T. & Akella, J. (2001) *J. Nanosci. Nanotechnol.* **1,** 143–147.
15. Reich, S., Thomsen, C. & Ordejon, P. (2002) *Phys. Rev. B Condens. Matter* **65,** 153407.
16. Venkateswaran, U. D., Rao, A. M., Richter, E., Menon, M., Rinzler, A., Menon, R. E. & Eklund, P. C. (1999) *Phys. Rev. B Condens. Matter* **59,** 10928–10934.
17. Tang, J., Qin, L. C., Sasaki, T., Yudasaka, M., Matsushita, A. & Iijima, S. (2002) *J. Phys. Condens. Matter* **14,** 10575–10578.
18. Brazhkin, V. V., Lyapin, A. G. & Hemley, R. J. (2002) *Phil. Mag. A* **82,** 231–253.
19. Yan, C. S., Mao, H. K., Li, W., Qian, J., Zhao, Y. & Hemley, R. J. (2004) *Phys. Stat. Sol. A* **201,** 25–27.